Progress In Electromagnetics Research Letters, Vol. 80, 149–157, 2018

A Dual-Polarized Omnidirectional Antenna with Two Kinds of Printed Wideband Low-Profile Radiating Elements

Yuwei Zhang, Shu Lin*, Shang Yu, Shoulan Liu, Guanjun Liu, and Alexander Denisov

Abstract—This paper describes a printed wideband low profile omnidirectional dual-polarized antenna, which is a combination of vertical polarization (VP) and horizontal polarization (HP) elements. The VP element printed on a double-layered disk-shaped substrate is a modified monopole with loadings. The introduction of the material of the dielectric substrate can reduce the profile height in the polarized direction to $0.08\lambda_L$ (the wavelength at the lowest frequency). And loading metallic cylindrical block and shorting-posts in the dielectric substrate to improve the bandwidth are realized by using metal-vias. The HP element consists of a printed 8-element circular connected Vivaldi antenna array, and each element contains a director in the slot for the improvement of radiation pattern's out-of-roundness. Both the simulated and measured results indicate that operating bands of 2.2–4.52 GHz for VP and 2.4–3.8 GHz for HP. This proposed antenna has good isolation and omnidirectional patterns with the out-of-roundness less than 2.5 dB in the azimuth plane for both VP and HP, and it can be applied in mobile communication systems.

1. INTRODUCTION

Due to the property of 360° full coverage radiation in the horizontal plane and supporting a free alignment between receiving and transmitting antennas, omnidirectional antennas have drawn tremendous attention in modern wireless communication systems, such as base stations, indoor distributed antenna system (IDAS), WLANs, and mobile terminal devices [1–5]. On the other hand, dual-polarized antennas, which have two orthogonal electrical field components in the radiating direction, with the advantages of enhancing spectrum efficiency and mitigating polarization mismatch between receiver and transmitter are also suitable for modern wireless communication systems. According to above facts, the designs of omnidirectional dual-polarized antennas with compact size, low profile (lower height of its profile), wide band and good port isolation are facing technical challenges. Recently, a lot of dual-polarized omnidirectional antennas have been designed with diverse radiation structures. In [6], an omnidirectional dual-polarized antenna with compact size of 83 mm × 11 mm × 11 mm is achieved by cutting two colocated slots on the walls of a slender columnar, and it is designed for 2.4 GHz WLAN with the operating band of 9.5%. Another omnidirectional dual-polarized antenna designed by modifying the antenna in [6] is presented in [7], and the antenna volume is reduced to 42 mm × 12 mm × 12 mm; however the bandwidth is still narrow of 15%. The antenna composed of an annular-ring patch for vertical polarization (VP) and four curved branches for horizontal polarization (HP) with the low profile of 4 mm is proposed in [8], but the bandwidth is not more than 9%. In [9], a novel structure of four pairs of orthogonal dipoles is presented for an omnidirectional dual-polarized antenna which can achieve 30% bandwidth with the port isolation about 25 dB, and the profile height can reach 100 mm. In the light of the current literature, the common method to obtain omnidirectional dual-polarized antenna is combining different VP and HP antennas [10–15], among which modified monopoles are used for VP elements, while printed circular

Received 19 November 2018, Accepted 14 December 2018, Scheduled 28 December 2018
* Corresponding author: Shu Lin (linshu@hit.edu.cn).
The authors are with the Harbin Institute of Technology, China.

loop antennas or concentrically arranged dipoles are designed for the HP elements. These antennas can cover wide operating band, but the profile heights of VP elements are not lower than $0.12\lambda_L$. In addition, as the same kind of antenna as above, [16] adopts an AMC reflector to decline the profile height, which sacrifices the port isolation to 20 dB. [17] employs a novel three-element wideband and high-gain electromagnetic structure (WHEMS) for HP element; however, its profile height is still large of 100 mm.

In this paper, a broadband low profile omnidirectional dual-polarized printed antenna is proposed. It is a combination of a vertical polarization (VP) antenna and a horizontal polarization (HP) antenna. The VP antenna is designed on the base of the previous work [18], and the HP antenna is composed of eight concentrically arranged Vivaldi antennas with parasitic patches. This antenna achieves omnidirectional radiation property in both the VP and HP elements, and in the radiating direction, two orthogonal electrical field components are available which means that this antenna owns a dual-polarization characteristic. The height in the profile of only 52.7 mm validating low profile can be achieved by introducing dielectric substrates into both VP and HP elements. And the bandwidths are wide of 69% for VP and 45.2% for HP. Good port isolation larger than 35 dB at the overlapping frequency band is obtained. This antenna design can be used for base station, IDAS, WLAN and 5G wireless communication systems. Detailed antenna design and analysis are depicted in Section 2; the simulation and measurement are presented in Section 3, while the conclusion are provided in Section 4.

2. ANTENNA GEOMETRY AND DESIGN

2.1. VP Element

As shown in Figure 1, between the top circular patch and ground plane, which are both printed on the surface of the substrate, the metal cage instead of cylindrical block, the inner feed probe, and seven

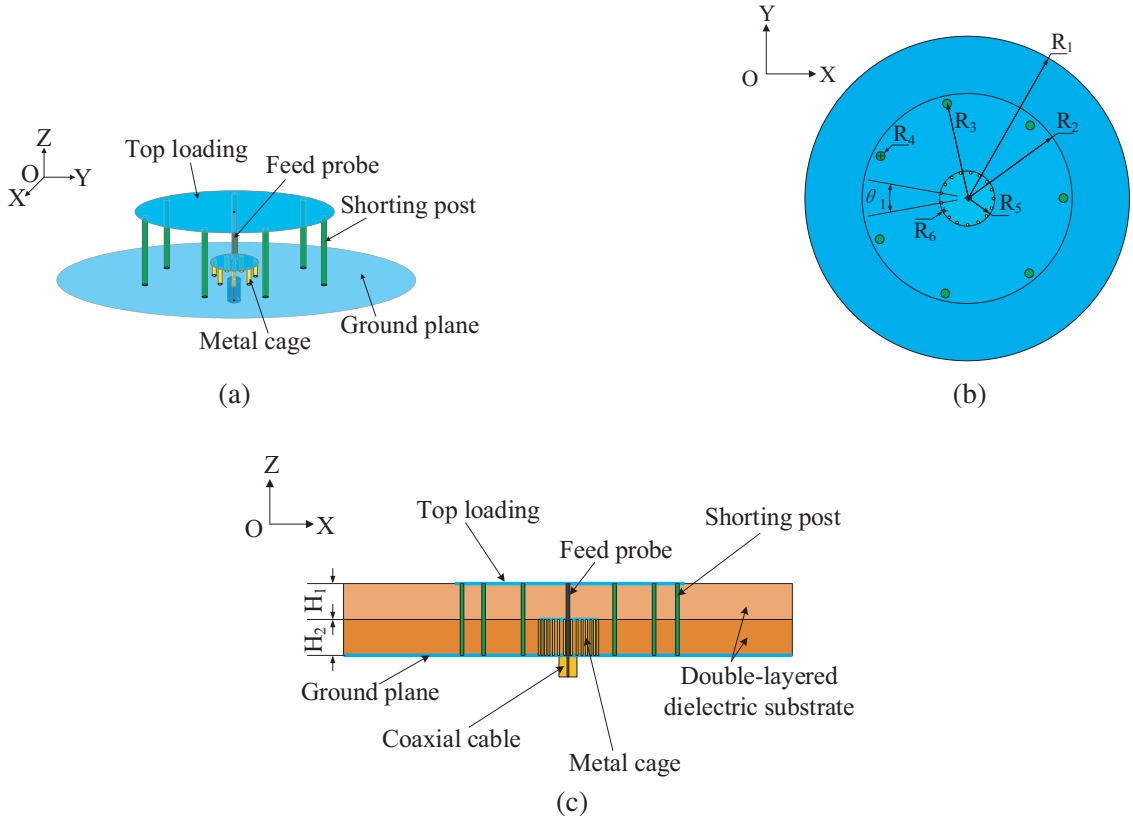

Figure 1. Geometry of the VP element. (a) Perspective view (hiding the substrate). (b) Top view. (c) Side view.

shorting posts are situated in the double-layered substrate ($\varepsilon_r = 3.5$ and thickness = 11 mm). The initial designed antenna is a monopole loaded with a metal cylindrical block on the ground plane, and in order to reduce the profile height, a top-loading circular patch, which can extend the electrical length, is mounted above the ground plane with a distance, while the impedance bandwidth cannot satisfy our requirement under such a case. For bandwidth improvement, 7 equally-spaced metallic posts, which short the top-loading to the ground, are exploited to compensate the reactance. Moreover, a double-layered cylinder dielectric served as the printed circuit board is introduced between the top-loading and ground plane that can cause the working frequency altered from f_0 to $\frac{f_0}{\sqrt{\varepsilon_e}}(1 < \varepsilon_e < \varepsilon_r)$, and at the same time, all the antenna radiation portions are printed on it.

The evolutionary process with corresponding equivalent circuits of the proposed VP antenna is demonstrated in Figure 2. X_1–X_3 are corresponding reactance components of the circuits generated by loading the new antenna structures termed as loading 1–loading 3. As seen, introducing a new structure in the antenna corresponds to adding an X in the equivalent circuit, and due to additions of these reactance components, the variables for adjusting the impedance matching are increased which means that the broadband impedance matching can be achieved easily. Moreover, concerning the property of circuitry, the loading of dielectric substrate can enhance the capacitance value without impacting the inductance value, resulting in lowering the resonance frequency.

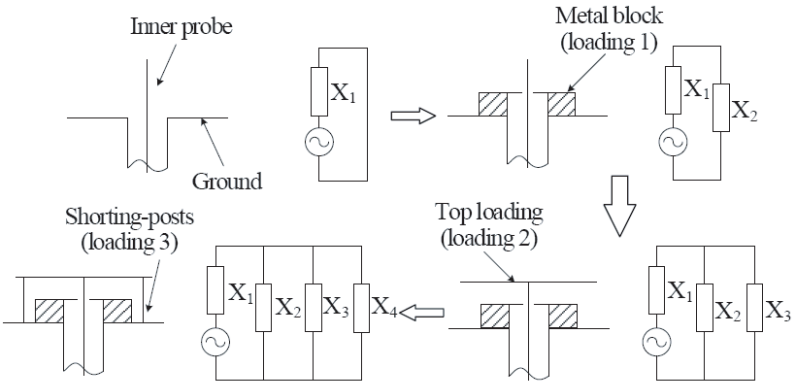

Figure 2. The evolutionary process with corresponding equivalent circuits of the proposed VP element.

Then, let us discuss key techniques of this antenna design by the following simulation results shown in Figure 3. Figure 3(a) gives the simulated reflection coefficient of the proposed VP antenna with/without the substrate. It is seen that the resonance frequency is shifted to the lower side by loading the dielectric substrate. Stated in another way, when the working frequency is fixed, the profile height can be reduced by introducing the substrates, and the impedance matching is also ameliorated by the dielectric substrate. To study the contribution of the shorting pins, the impedance curves with/without the seven-posts are plotted in Figure 3(b). When we load the pins, the impedance curve moves into the $\Gamma = 1/3$ circle on the Smith chart that indicates the impedance matching being improved. In other words, the bandwidth is broadened. The technology of metal vias, which are easy to fabricate and can reduce the antenna's weight, is adopted for realizing the loadings of metallic cylindrical surface and shorting posts in the dielectric substrate. Figure 3(c) shows the simulated results of $|S_{11}|$ and surface current distributions of the VP antenna with metal cage compared with metal block, and it is clear that the reflection coefficients and current distributions are almost the same in the two cases; therefore, using metal vias to replace the metal block is absolutely feasible.

The optimum dimensions of the VP element are listed in Table 1.

2.2. HP Element

As displayed in Figure 4, the HP element composed of a feeding network in the middle and eight concentrically arranged Vivaldi antenna elements is printed on both sides of the circular substrate

Table 1. Geometric parameters for VP antenna (Unit: millimeters).

R_1 (mm)	60	R_2 (mm)	33.7	R_3 (mm)	31.65	R_4 (mm)	0.55	R_5 (mm)	5.7
R_6 (mm)	0.215	θ_1 (°)	8	H_1 (mm)	5.08	H_2 (mm)	5.08	l (mm)	75

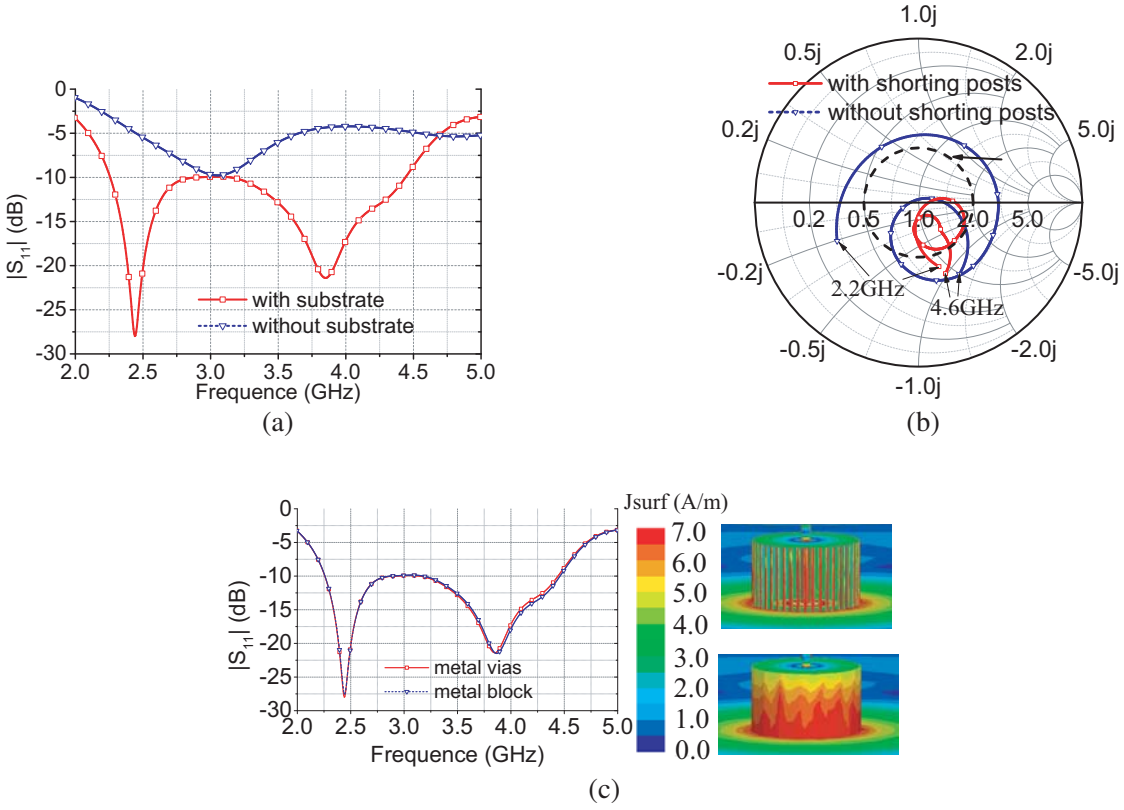

Figure 3. Simulated results of VP element. (a) Simulated reflection coefficient with/without the substrate. (b) Impedance curves with/without the seven-posts. (c) Simulated S_{11} and surface current distributions of the VP element with metal cage compared with metal block.

($\varepsilon_r = 2.2$ and thickness = 1.57 mm). Moreover, a quasi-trapezoid director is loaded in the slot of each Vivaldi element for the improvement of radiation pattern's out-of-roundness.

The profile of the exponential tapered slot shown in Figure 4 can be expressed as:

$$y_1 = 0.03e^{0.097x} + 0.15e^{0.09x} + 0.4 \tag{1}$$

And the eight pairs of taper microstrips, which can form an eight-way printed power divider to provide signals with equal amplitude and phase, are used for the connection between the coaxial cable and Vivaldi radiators, and the two profiles of the strip line can be written as:

$$y_2 = 2.01x^6 + 1 \tag{2}$$

$$y_3 = 2.96x \tag{3}$$

A metal disk connecting the strip lines to the coaxial line can obtain the expansion of the feeding lines to improve the power capacity of the antenna; however, that limits the bandwidth. Even so, the bandwidth of the HP element can match that of the VP antenna. A single Vivaldi antenna has directional radiation; therefore, using a Vivaldi antenna array to realize omnidirectional characteristic should determine the element number, and it can be obtained through the following formula:

$$2\pi\sqrt{(R/\lambda_{\min})/K} \leq N \leq 4\pi\sqrt{\varepsilon_e}R/\lambda_{\max} \tag{4}$$

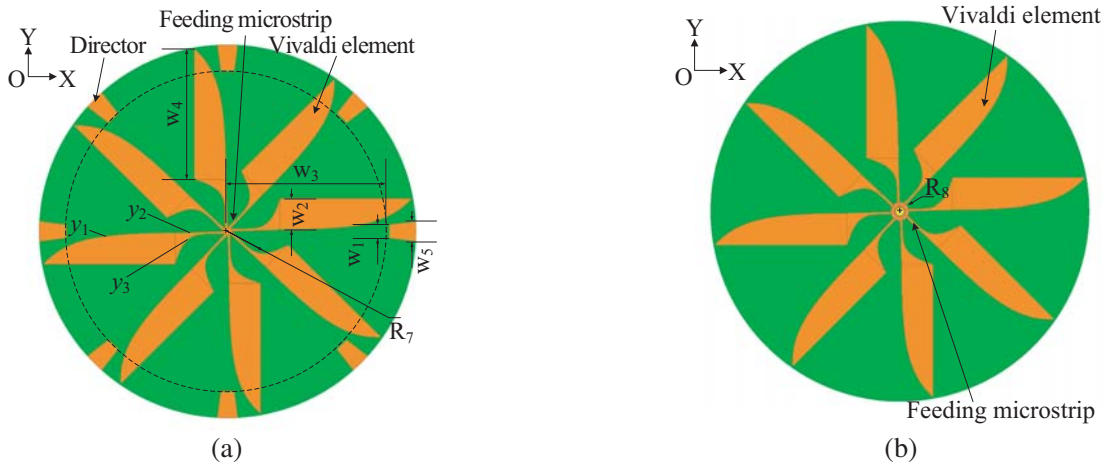

Figure 4. Geometry of the HP element. (a) Front view. (b) Back view.

where R is the radius of the circular substrate; $\lambda_{\min}/\lambda_{\max}$ is the lowest/highest working wavelength; K is the coefficient determined by the aperture-field with the range of $0.89 \leq K \leq 1.19$, where 0.89 and 1.19 correspond to uniform distribution aperture and cosine distribution aperture, respectively. Firstly, according to the boundary of the VP operating band, the values of $\lambda_{\max}$ and $\lambda_{\min}$ are attained. Then, to ensure good impedance matching for a broadband, the longitudinal dimension of the single Vivaldi element which decides the matching characteristic should be larger than $\lambda_{\max}/2$ [19], while the value of R depends on the longitudinal dimension. Moreover, considering the area of the feeding network, the optimum radius is set to $R = 70\,\text{mm}$ after simulation. Finally, by taking these parameters into formula (4), we can calculate $N = 8$. To investigate how the quasi-trapezoid director affects the out-of-roundness, Figure 5 gives the HP element radiation pattern at 2.7 GHz when the directors are appended or not. It can be observed that when the directors are added, the out-of-roundness of the omnidirectional radiation pattern will be ameliorated by 0.75 dB from $-2.5\,\text{dB}$ to $-1.75\,\text{dB}$. The optimum dimensions of the HP element are listed in Table 2.

Table 2. Geometric parameters for HP antenna (Unit: millimeters).

w_1 (mm)	7.64	w_2 (mm)	11.35	w_3 (mm)	60.5	w_4 (mm)	49.4
w_5 (mm)	7.6	R_7 (mm)	70.5	R_8 (mm)	3.35	-	-

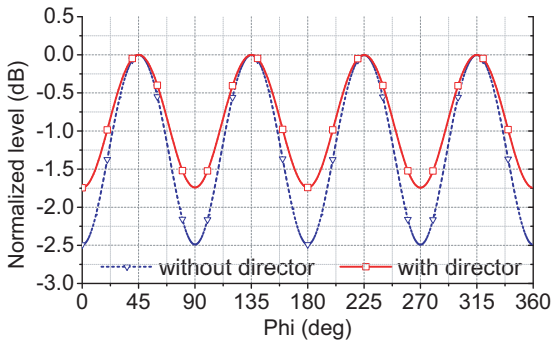

Figure 5. The simulated radiation pattern at 2.7 GHz of the HP element with/without the directors.

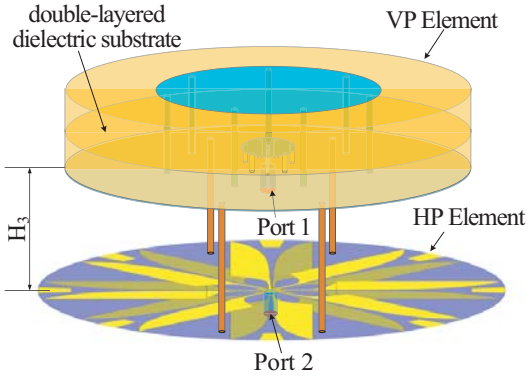

Figure 6. Geometry of the proposed dual-polarized antenna.

2.3. Dual-polarized Omnidirectional Antenna

By placing the VP antenna above the HP antenna with a distance, the dual-polarized antenna, as shown in Figure 6, is accomplished, and the two elements are fed separately. Due to the influence from the ground plane of the VP element, the current distribution of the HP element is changed compared with the isolated HP antenna, which leads to the variation of the impedance matching. Moreover, the impact will be stronger when the two elements get closer, which can be noted from the simulated $|S_{11}|$ results of the combined dual-polarized antenna, shown in Figure 7, whereas, the VP element is almost not affected by the ground plane and the HP element beneath it. Meanwhile, in order to achieve lower profile height, the distance between the two elements should be as close as possible. Thus, considering the above mentioned situations, we choose 37 mm for the distance of H_3.

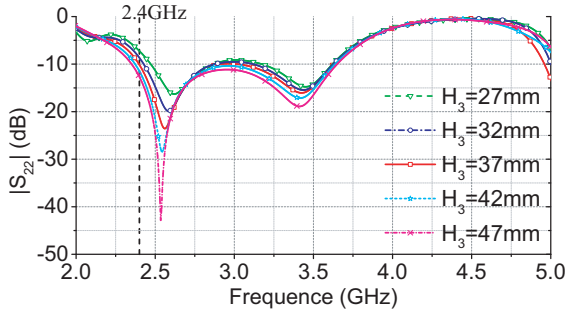

Figure 7. Simulated results of $|S_{22}|$ of the proposed dual-polarized antenna with different H_3.

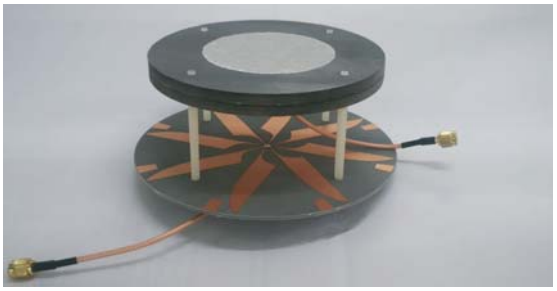

Figure 8. Prototype of the proposed dual-polarized antenna.

3. RESULT AND DISCUSSION

A prototype of the proposed dual-polarized antenna, as exhibited in Figure 8, is fabricated. VP and HP elements are printed on a double-layered F4BTM-2 dielectric substrate ($\varepsilon_r = 3.5$, $\tan\delta = 0.002$, thickness = 11 mm) and a F4BM-2 dielectric substrate ($\varepsilon_r = 2.2$, $\tan\delta = 0.001$, thickness = 1.57 mm), respectively. Both of them are fed by 50 Ω coaxial cables, and four dielectric cylinders of 37 mm height are mounted between the two elements for supporting. This proposed antenna is measured in an anechoic chamber by the Agilent N5227A vector network analyzer.

Figure 9 displays the simulated and measured results of S-parameters. It can be found that, for VP element, the simulated −10-dB impedance bandwidth is from 2.26 to 4.54 GHz and the measured one from 2.2 to 4.52 GHz. The simulated and measured −10-dB impedance bandwidths for HP element

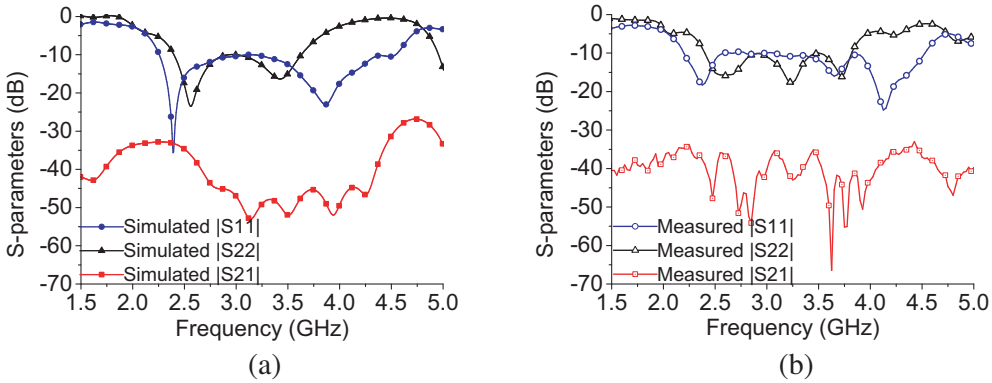

Figure 9. (a) Simulated and (b) measured S-parameters of the proposed antenna.

are from 2.4 to 3.63 GHz and from 2.4 to 3.8 GHz, respectively. Additionally, the ports isolation in the overlapping operating band is larger than 33 dB for simulation and 35 dB for measurement. The minor differences between the simulation and measurement results are caused by the loss of feeding network, error of fabrication, and influence of experiment environment.

The measured radiation patterns of the proposed antenna are shown in Figure 10. It can be observed that both the VP and HP antennas can achieve omnidirectional radiation characteristic in horizontal plane, and the out-of-roundnesses of these omnidirectional patterns are less than 3 dB. There is some tilt of the maximum radiation directions of both VP and HP in the vertical plane, caused by the reflection of the VP's ground plane.

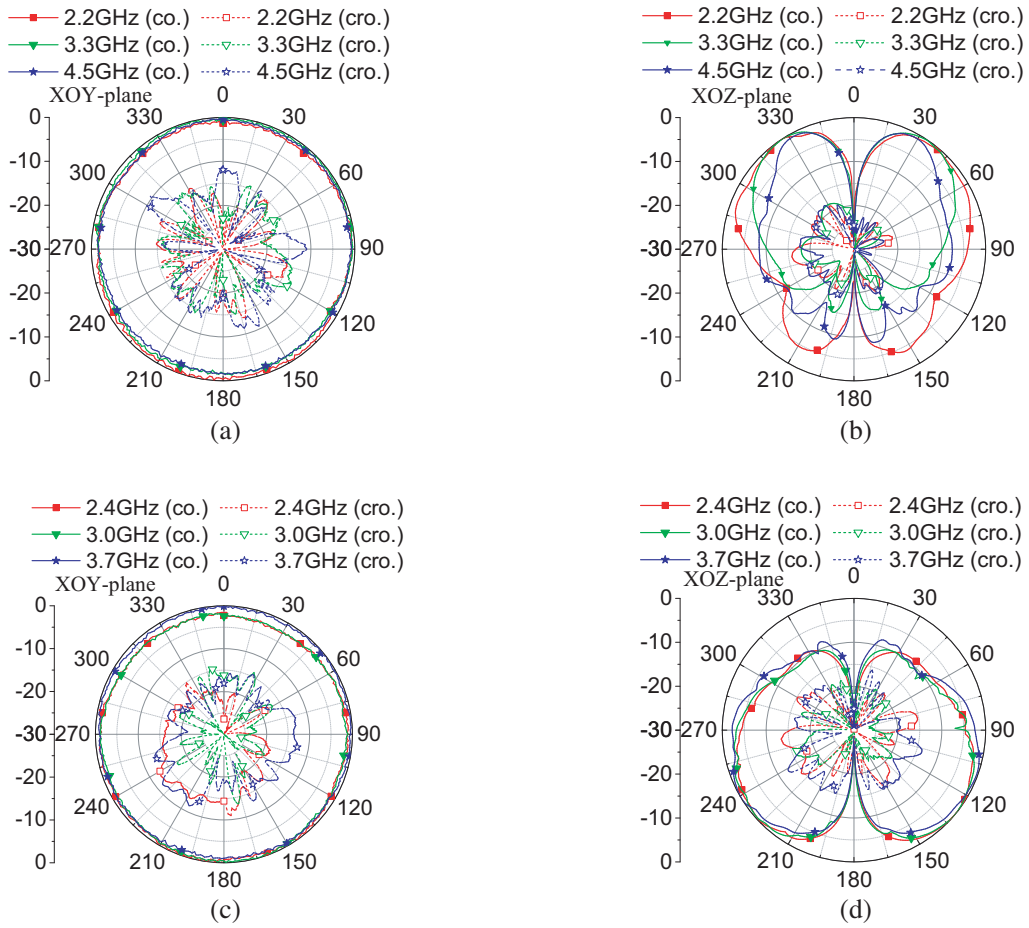

Figure 10. Measured radiation patterns of the proposed antenna. (a) XOY-plane for VP. (b) XOZ-plane for VP. (c) XOY-plane for HP. (d) XOZ-plane for HP.

Figure 11 gives the gains and radiation efficiencies of the proposed antenna. The simulated and measured gains ranging from 3.3 to 3.8 dBi of HP antenna coincide well with each other, while the simulated gain of VP antenna varies from 3.0 to 7.3 dBi, and the measured gains range from 3.1 to 7.1 dBi. The little difference between them is due to the losses of the dielectric substrate and feeding network, and also caused by the measurement environment. In addition, the simulated radiation efficiencies better than 89.4% are attained for VP and HP elements.

Table 3 shows the comparison between the proposed antenna and other antennas. All these antennas are designed by a similar methodology which combines VP and HP antennas to attain wideband dual-polarized omnidirectional antennas. As seen in Table 3, the proposed dual-polarized antenna has the lowest profile height of VP element because of employing the dielectric substrate. In addition, it also has relatively low profile for the entire structure, good isolation and wide bandwidth.

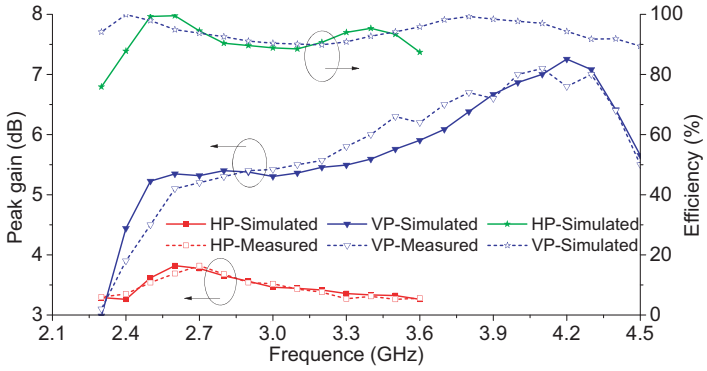

Figure 11. The peak gains and radiation efficiency of the proposed dual-polarized antenna.

Table 3. Comparison between the proposed antenna and other antennas.

Ref.	Profile Height	Bandwidth (VP)	$\frac{H_{\rm VP}}{\lambda_L}$*	Bandwidth (HP)	Isolation
[10]	77.8 mm	0.86–5.62 GHz (200%)	0.16	1.62–2.71 GHz (50.3%)	Higher than 26 dB
[11]	102.6 mm	0.671–3.58 GHz (137%)	0.12	1.7–3 GHz (55%)	Higher than 25 dB
[12]	35 mm	1.7–3.5 GHz (69%)	0.15	2.03–2.71 GHz (28.7%)	Higher than 30 dB
[13]	67 mm	1.68–2.72 GHz (47.3%)	0.12	1.7–2.80 GHz (48.9%)	Higher than 25 dB
[14]	72 mm	1.7–2.2 GHz (25%)	0.15	1.7–2.2 GHz (25%)	Around 40 dB
[15]	85 mm	0.8–2.7 GHz (108%)	0.12	1.7–2.7 GHz (45.5%)	Higher than 38 dB
Proposed Antenna	52.7 mm	2.2–4.52 GHz (69%)	0.08	2.4–3.8 GHz (45.2%)	Higher than 35 dB

*$H_{\rm VP}$ — the profile height of VP element.
λ_L — the wavelength of the lowest operating frequency.

4. CONCLUSION

A printed wideband low profile omnidirectional dual-polarized antenna is presented in this paper. The proposed antenna uses a VP element and an HP element to achieve dual polarizations. Because of the introduction of dielectric substrate, the profile height of VP element can be only $0.08\lambda_L$, and its bandwidth can reach 69% by the loadings. For HP element, a Vivaldi antenna array is applied to omnidirectional radiation, and its bandwidth can reach 45.2%. Good port isolation of larger than 35 dB at the overlapping frequency band is attained, and omnidirectional radiation patterns are achieved in XOY-plane for both of the antenna elements with the out-of-roundness less than 2.5 dB. The peak gains can reach 7.1 dBi for VP and 3.8 dBi for HP. Also, this antenna has better radiation efficiencies in the whole operation bands. With such merits, this antenna is suitable for the applications of base station, IDAS, WLAN and 5G wireless communication systems.

ACKNOWLEDGMENT

This work was supported in part by the Natural Science Foundation of Heilongjiang Province under Grant F2017011. The authors would also like to thank CST Ltd. Germany, for providing the CST Training Center (Northeast China Region) at our university with a free package of CST MWS software.

REFERENCES

1. Wang, J., L. Zhao, Z. C. Hao, and J. M. Jin, "A wideband dual-polarized omnidirectional antenna for base station/WLAN," *IEEE Transactions on Antennas and Propagation*, Vol. 66, No. 1, 81–87, 2017.

2. Kim, S. C., S. H. Lee, and Y. S. Kim, "Multi-band monopole antenna using meander structure for handheld terminals," *Electronics Letters*, Vol. 44, No. 5, 331–332, 2008.
3. Yang, N., K. W. Leung, K. Lu, and N. Wu, "Omnidirectional circularly polarized dielectric resonator antenna with logarithmic spiral slots in the ground," *IEEE Transactions on Antennas and Propagation*, Vol. 64, No. 2, 796–800, 2016.
4. Svezhentsev, A. Y., V. Volski, and S. Yan, "Omnidirectional wideband E-shaped cylindrical patch antennas," *IEEE Transactions on Antennas and Propagation*, Vol. 65, No. 2, 839–844, 2017.
5. Bhadoria, B. and S. Kumar, "A novel omnidirectional triangular patch antenna array using dolph chebyshev current distribution for C-band applications," *Progress In Electromagnetics Research M*, Vol. 71, 75–84, 2018.
6. Li, Y., Z. Zhang, J. Zheng, and Z. Feng, "Compact azimuthal omnidirectional dual-polarized antenna using highly isolated colocated slots," *IEEE Transactions on Antennas and Propagation*, Vol. 60, No. 9, 4037–4045, 2012.
7. Li, Y., Z. Zhang, Z. Feng, and M. F. Iskander, "Design of omnidirectional dual-polarized antenna in slender and low-profile column," *IEEE Transactions on Antennas and Propagation*, Vol. 62, No. 4, 2323–2326, 2014.
8. Deng, C., P. Li, and W. Cao, "A high-isolation dual-polarization patch antenna with omnidirectional radiation patterns," *IEEE Antennas and Wireless Propagation Letters*, Vol. 11, No. 6, 1273–1276, 2013.
9. Fan, Y., X. Liu, B. Liu, and R. L. Li, "A broadband dual-polarized omnidirectional antenna based on orthogonal dipoles," *IEEE Antennas and Wireless Propagation Letters*, Vol. 15, No. 2, 1257–1260, 2016.
10. Yu, L., J. Song, Y. Gao, K. He, and F. Gao, "Low-profile dual-polarized omnidirectional antenna for broadband indoor distributed antenna system," *Progress In Electromagnetics Research Letters*, Vol. 67, 39–45, 2017.
11. Jolani, F., Y. Yu, and Z. Chen, "A novel broadband omnidirectional dual polarized MIMO antenna for 4G LTE applications," *IEEE Wireless Symposium*, 1–4, 2014.
12. Bai, X., M. Su, Z. D. Gao, and Y. A. Liu, "Broadband dual-polarized omnidirectional antenna based on magnetic dipoles," *IEICE Electronics Express*, Vol. 15, No. 5, 1–8, 2018.
13. Yu, Y., H. Zhang, and Z. Chen, "A broadband dual-polarized omnidirectional MIMO antenna for 4G LTE applications," *Progress In Electromagnetics Research Letters*, Vol. 57, 91–96, 2015.
14. Quan, X. L. and R. L. Li, "A broadband dual-polarized omnidirectional antenna for base stations," *IEEE Transactions on Antennas and Propagation*, Vol. 61, No. 2, 943–947, 2013.
15. Zhou, L., Y.-C. Jiao, Z.-B. Weng, Y. Qi, and T. Ni, "Wideband dual-polarized omnidirectional antenna with high isolation for indoor DAS applications," *Progress In Electromagnetics Research C*, Vol. 61, 105–113, 2016.
16. Wu, J., S. Yang, Y. Chen, S. Qu, and Z. Nie, "A low profile dual-polarized wideband omnidirectional antenna based on AMC reflector," *IEEE Transactions on Antennas and Propagation*, Vol. 65, No. 1, 368–374, 2017.
17. Wen, H., Y. Qi, Z. Weng, F. Li, and J. Fan, "A multiband dual-polarized omnidirectional antenna for 2G/3G/LTE applications," *IEEE Antennas and Wireless Propagation Letters*, Vol. 17, No. 2, 180–183, 2017.
18. Lin, S., G. J. Liu, Y. W. Zhang, H. Zong, S. Qiu, S. C. Lan, and A. Denisov, "A low-profile vertical polarized omnidirectional radiated and broadband printed antenna," *IEEE International Symposium on Antennas Propagation*, 1801–1802, Jul. 2016.
19. Pozar, D. M., *Microwave Engineering*, 4th edition, Wiley, 2005.